JACS
JOURNAL OF THE AMERICAN CHEMICAL SOCIETY

Communication

pubs.acs.org/JACS

Rapid, Large-Area Synthesis of Hierarchical Nanoporous Silica Hybrid Films on Flexible Substrates

Dong-Po Song, Aditi Naik, Shengkai Li, Alexander Ribbe, and James J. Watkins*

Department of Polymer Science and Engineering, University of Massachusetts Amherst, 120 Governors Drive, Amherst, Massachusetts 01003, United States

Supporting Information

ABSTRACT: We report a simple strategy for the creation of large-area nanoporous hybrid films of silica, carbon, and gold on polyethylene terephthalate via photothermal processing. This method enables the selective heating of light-absorbing thin films on low-temperature substrates using sub-millisecond light pulses generated by a xenon flash lamp. The film contains gold nanoparticles as the nanoheaters to convert light energy to heat, a sacrificial block copolymer surfactant to generate mesopores, and cross-linked polyhedral oligomeric silsesquioxane as the silica source to form the skeleton of the porous structure. Hierarchical porous structures are achieved in the films after photothermal treatment, with uniform mesopores (44−48 nm) on the surface and interconnected macropores (>50 nm) underneath resulting from a foaming effect during release of gaseous decomposition products. The loading of gold nanoparticles is up to 43 wt % in the product, with less than 2 wt % organic residue. This rapid and large-area process for the synthetis of porous structures is compatible with roll-to-roll manufacturing for the fabrication of flexible devices.

Hierarchical nanoporous hybrid materials containing functional nanoparticles (NPs) are important for a range of applications, including catalysis, separation, sensing, and energy storage and conversion.[1−7] The pore size within these materials can be manipulated through the self-assembly of sacrificial soft templates including, small molecular surfactants and block copolymers (BCPs).[8−21] Typically, time-consuming multiple steps are required for the preparation of mesoporous hybrids containing functional NPs such as noble metals and magnetic metal oxides.[22,23]

Rapid preparation of large-area hierarchical nanoporous films on flexible substrates will not only enable the fabrication of lightweight and portable devices but also reduce the fabrication cost by allowing large-scale manufacturing methods, such as roll-to-roll processing. However, conventional synthetic methods to form porous structures usually require furnace calcinations of the materials at temperatures of more than 400 °C for several hours, leading to the degradation of polymer-based substrates.[9−23] Recently, laser beam writing has been used in the synthesis of porous materials, providing an alternative thermal processing method to enable direct pattern transfer.[24,25] For example, Tan et al. prepared nanoporous carbon using laser-induced transient heating of a BCP mixture on silicon substrate followed by furnace carbonization.[24] Here, the substrate absorbs light energy and converts the mixture film into a porous polymeric resin. Lin et al. reported a one-step approach for producing patterned porous graphene films from commercial polymer films using a CO_2 infrared laser.[25] However, it is challenging to fabricate large-area hierarchical porous films on a short time scale using a laser due to the limited beam size. Therefore, the development of efficient methods for the rapid and large-area synthesis of nanoporous films remains of great interest.

We demonstrate a simple method to realize the rapid and large-area synthesis of hierarchical nanoporous hybrid films of silica, carbon, and gold on a commercially available polyethylene terephthalate (PET) substrate via photothermal processing. As shown in Scheme 1, the light-absorbing thin film contains gold NPs as the nanoheaters to convert light energy to heat via strong localized surface plasmon resonance (LSPR), a sacrificial (polynorbornene-*graft*-polystyrene)-*block*-(polynorbornene-*graft*-poly(ethylene oxide)) (PS-*b*-PEO) brush BCP to create mesopores, and cross-linked polyhedral oligomeric silsesquioxane (POSS) as the silica source to form the skeleton of the porous structure. The PS-*b*-PEO brush BCP

Scheme 1. Illustration of a Rapid and Scalable Process for the Synthesis of Hierarchical Porous Hybrid Films of Silica, Carbon, and Gold on PET via Photothermal Treatment[a]

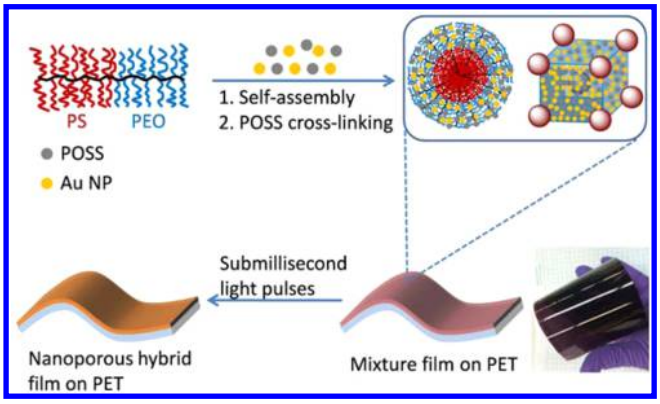

[a]Both POSS and gold NPs are selectively incorporated within the PEO domain of a self-assembled PS-*b*-PEO brush BCP via hydrogen bonding.

Received: July 5, 2016
Published: October 5, 2016

DOI: 10.1021/jacs.6b06947
J. Am. Chem. Soc. 2016, 138, 13473−13476

(M_n = 1583 kg/mol, PDI = 1.06, f_{PEO} = 48.4 wt %) was synthesized by sequential ring-opening metathesis polymerization according to our reported synthetic procedure (Figures S1 and S2).[26,27] The molecular weights of the PS and PEO side chains are 3.5 and 2.0 kg/mol, respectively. Gold NPs with diameter of ~2 nm were coated with 4-mercaptophenol, which exhibits strong hydrogen-bonding interactions with the PEO domain (Figure S3).[27] The thin film was prepared over large areas by rod coating and by thermal annealing to enable the ripening of NPs to larger sizes (>10 nm) as well as to initiate cross-linking of POSS (see Supporting Information).[27,28] As shown in Figure 1a, a strong LSPR peak at 543 nm was

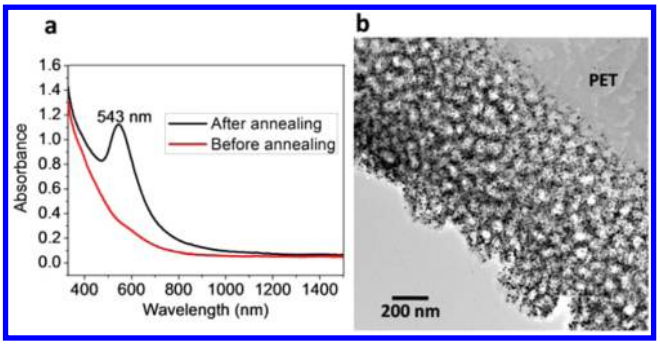

Figure 1. (a) Absorption spectra of the mixture coating film on PET before and after thermal annealing at 120 °C for 20 h. (b) Bright-field cross-sectional TEM micrograph of the film after annealing. The average thickness of the film is ~920 nm. No staining was applied.

observed after annealing, providing high light-absorbing efficiency in the film for subsequent photothermal processing. For comparison, no obvious LSPR can be indentified for the unannealed sample (Figure 1a) containing small NPs (2 nm).[29] Cross-linking of POSS cages was achieved via imide formation between carboxylic acid and secondary amine groups on POSS upon heating,[28] which was verified by Fourier-transform infrared spectroscopy (FTIR) (Figure S4). Sphere-like morphologies were formed via self-assembly during solvent evaporation, with PS appearing as the spheres and gold NP/POSS-incorporated PEO domain as the matrix (see Scheme 1). This was confirmed by small-angle X-ray scattering (SAXS), field emission scanning electron microscopy (FESEM) (Figure S5), and cross-sectional trasmission electron microscopy (TEM) of thin sections from the annealed sample (Figure 1b). Because PS and PEO in unstained samples have similar electron densities, the contrast observed in the TEM image is due to the gold NPs and POSS residing exclusively in PEO domains (Figure 1b).[26,27,30] The domain spacing of the spherical structure is ~84 nm, as determined by SAXS (Figure S5). To create well-defined porous structures, the BCP template is removed, and the cross-linked POSS matrix is oxidized to silica upon heating.[31]

For the photothermal processing, the emission of light is in a wide wavelength range from 200 to 1000 nm, with the peak intensity between 400 and 500 nm (Figure S6). The light intensity is precisely tunable through the variation of voltage and/or pulse duration time. The optimal process includes three repeats of a same pulse with a duration of 0.3 ms (see Supporting Information). Figure 2a shows FTIR spectra of four representative samples: control sample without photothermal processing and samples 1−3 obtained using pulse energies of 1785, 1837, and 1891 mJ/cm^2, respectively. The multiple

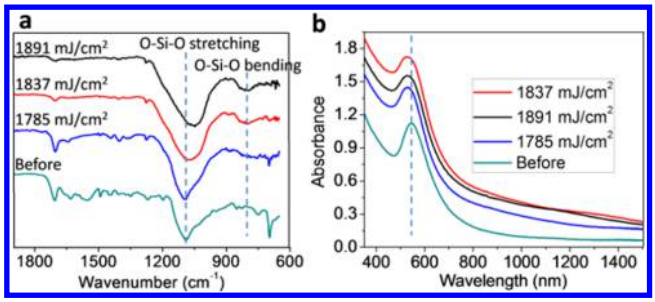

Figure 2. (a) FTIR spectra of the films before and after photothermal treatments under different light pulse energies. (b) Absorption spectra of these samples, showing strong LSPR of the gold NPs.

absorption peaks in the range from 1800 to 1200 cm^{-1} are ascribed to organic components and gradually disappeared with increasing pulse energy. The removal of organics was also confirmed by the absence of peaks in the range from 3100 to 2800 cm^{-1}, corresponding to C−H stretch (Figure S7). A blue shift of the O−Si−O stretching peak was observed as the pulse energy increased, indicating the opening and oxidation of POSS cages to a network-like silica structure (Figure 2a).[31] In contrast, no evident changes in FTIR and no evidence of a nanoporous structure in FESEM images were observed for samples without gold exposed to the xenon flash lamp using the same pulse energies (Figure S8), suggesting that the gold NPs enabled the conversion of light energy to heat for the creation of nanoporous structures. The oxidation of POSS was further confirmed by a small change in the binding energy of the 2p orbital of silicon between the control sample and sample 3 (102.2 vs 103.0 eV) according to X-ray photoelectron spectroscopy (XPS) (Figure S9). Table 1 shows the

Table 1. Compositions of Representative Samples Prepared Using Different Pulse Energies[a]

sample	voltage (V)	pulse energy (mJ/cm^2)	silica or POSS (wt %)	carbon (wt %)	gold (wt %)	organic residue (wt %)
control	0	0	11.2	0	23.3	65.5
1	475	1785	32.0	14.0	45.9	8.10
2	480	1837	33.6	15.4	46.7	4.32
3	485	1891	37.3	18.0	43.0	1.70

[a]The weight percentage is calculated on the basis of the weight ratio of each component of the control sample or XPS data of the samples after photothermal treatment.

compositions of each sample as verified by XPS, and the corresponding atomic ratios are summarized in Table S1. Generally, there are significant increases in the weight percentages of silica (11.2 vs 37.3 wt %), carbon (0 vs 18.0 wt %), and gold NPs (23.3 vs 43.0 wt %) with increased pulse energy, while a remarkable decrease of organic residues was observed, from 65.5 to 1.70 wt % (Table 1), indicating the high efficiency of our synthetic method. It is worth noting that an abnormal increase of silica weight percentage was observed when the pulse energy was changed from 1837 to 1891 mJ/cm^2 (see Table 1). This can be best explained by the large number of POSS cages oxidized in air at a higher light intensity, which is consistent with an evident blue shift of the O−Si−O stretching peak oberved in FTIR (Figure 2a), as well as the XPS data (Figure S9).[28,31] This is also the reason why gold weight percentage decreased from 46.7 to 43.0 wt % (Table 1).

DOI: 10.1021/jacs.6b06947
J. Am. Chem. Soc. 2016, 138, 13473−13476

The efficient oxidation of POSS cages enables the creation of highly porous hybrid materials with good mechanical properties. In addition, the hybrid materials containing high concentrations of gold NPs exhibit strong LSPR, which is useful for many potential applications including, sensing (Figure 2b). A blue shift of the LSPR peak was observed for samples after photothermal treatments indicating the high sensitivity of gold NPs to their surrounding chemical evironment (organics vs air/silica/carbon), which is promising for sensor applications.[32]

The porous structures of samples 1−3 were characterized by FESEM and TEM (Figure 3). The FESEM micrographs

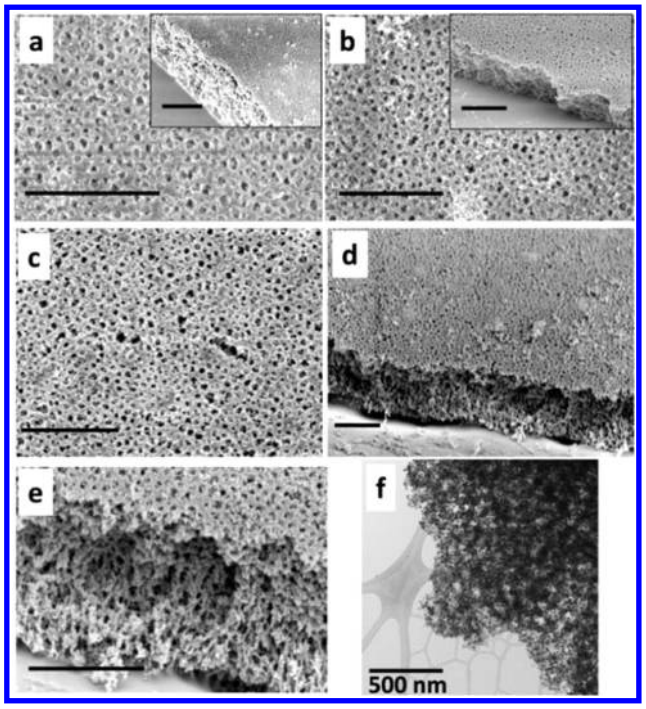

Figure 3. (a−e) FESEM micrographs of the samples 1−3 treated with different pulse energies, showing the structures of surface areas as well as cross sections: (a) sample 1 (1785 mJ/cm^2) with an average pore size on the surface of 44 ± 12 nm; (b) sample 2 (1837 mJ/cm^2) with an average pore size on the surface of 44 ± 9.5 nm; (c−e) sample 3 (1891 mJ/cm^2) with an average pore size on the surface of 48 ± 13 nm. The scale bars in the FESEM micrographs correspond to 1 μm. (f) Bright field cross-sectional TEM micrograph of sample 3 (1891 mJ/cm^2), showing a high loading of gold NPs.

showing large surface areas of these samples together with pore size distributions are given in Figure S10. The pore size was obtained via image analysis of more than 400 pores using ImageJ software. Impressively, well-controlled uniform pores ranging from ∼44 to 48 nm were formed on the surface of the resulting hybrid coatings during a rapid photothermal processing on the order of millisecond scale (Figure 3a−c). For comparison, a random porous structure was observed in a sample prepared using a PEO homopolymer as the template (see details in Figure S11), suggesting that the nanoporous sctructure was formed via replicating the sphere-like morphology of the self-assembled BCP nanocomposites. More interestingly, a foam-like porous structure with interconnected macropores of more than 50 nm was observed under the surface of sample 3, as indicated by cross-sectional FESEM micrographs (Figure 3d,e). This likely results from the rapid liberation of gaseous products during photothermal processing.[24,25] A similar porous structure was also observed in some small cracked areas on the surface, where large amounts of gases were released (Figure S12). For comparison, material under the film surface is less porous for samples 1 and 2 (insets of Figure 3a,b). In addition, the connections between surface pores and the macropores below can be clearly seen in FESEM micrographs at high magnifications (Figures 3e and S13). The high loading of gold NPs (43.0 wt %) are well dispersed in the skeleton of the porous strucure, without aggregation (TEM in Figure 3f). The hierarchical porous structure with large surface pores obtained may facilitate the penetration of large biological molecules for separation or sensing applications.[33,34]

Energy-dispersive X-ray spectrometry (EDS) for TEM was used to further verify the elemental distribution in the porous structure of sample 3 (Figure 4). Figure 4a shows the high-

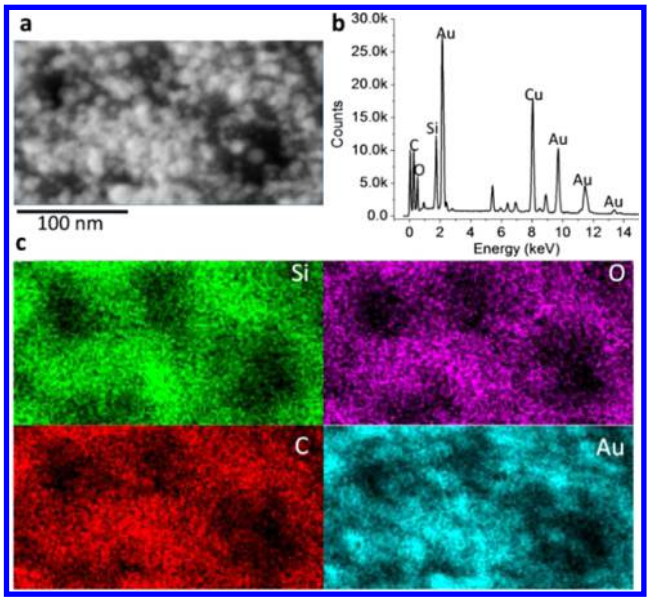

Figure 4. (a) HAADF-STEM micrograph of sample 3. (b) EDS spectrum of sample 3 showing elemental peaks corresponding to silicon, oxygen, carbon, and gold. (c) Elemental mapping of Si, O, C, and Au.

angle annular dark-field scanning TEM (HAADF-STEM) micrograph of an area for EDS mapping, where gold NPs appear as the bright regions in the image. Silicon, oxygen, carbon, and gold are confirmed in the EDS spectrum (Figure 4b), consistent with XPS results. Figure 4c shows the element maps in the porous structure, indicating a uniform distribution of all elements in the porous film, providing a route to hybrids with unique physical properties.

In summary, we have demonstrated a robust strategy for the synthesis of large-area nanoporous hybrid films on flexible substrates by rapid photothermal processing. This method enables the selective heating of only top coatings without damaging the underlying polymer substrate. In comparison with laser writing, this technique offers a great advantage in making large-area films, being compatible with roll-to-roll manufacturing. In addition, a hierarchical porous structure with large mesopores on the surface and foam-like macropores underneath was created in a short time of less than 1 ms. The hybrid films containing high concentrations of gold NPs in the unique porous structure may find applications in sensors and

DOI: 10.1021/jacs.6b06947
J. Am. Chem. Soc. 2016, 138, 13473−13476

catalysis. This strategy can be transferred to the synthesis of a variety of different porous hybrid films containing a broad range of functional additives that have high surface areas and well-controlled pore sizes for many applications, including supercapacitors, sensors, filtration, and catalysis.

■ ASSOCIATED CONTENT

Supporting Information

The Supporting Information is available free of charge on the ACS Publications website at DOI: 10.1021/jacs.6b06947.

Experimental information, Table S1, and Figures S1−S13 (PDF)

■ AUTHOR INFORMATION

Corresponding Author

*watkins@polysci.umass.edu

Notes

The authors declare no competing financial interest.

■ ACKNOWLEDGMENTS

This work was supported by the NSF Center for Hierarchical Manufacturing at the University of Massachusetts (CMMI-1025020).

■ REFERENCES

(1) Corma, A. *Chem. Rev.* **1997**, *97*, 2373.
(2) Davis, M. E. *Nature* **2002**, *417*, 813.
(3) Park, D.-H.; Nishiyama, N.; Egashira, Y.; Ueyama, K. *Ind. Eng. Chem. Res.* **2001**, *40*, 6105.
(4) Guliants, V. V.; Carreon, M. A.; Lin, Y. S. *J. Membr. Sci.* **2004**, *235*, 53.
(5) Liu, X.; Wang, R.; Xia, Y.; He, Y.; Zhang, T. *Sens. Lett.* **2011**, *9*, 698.
(6) Domansky, K.; Liu, J.; Wang, L.-Q.; Engelhard, M. H.; Baskaran, S. *J. Mater. Res.* **2001**, *16*, 2810.
(7) Aricò, A. S.; Bruce, P.; Scrosati, B.; Tarascon, J. M.; Van Schalkwijk, W. *Nat. Mater.* **2005**, *4*, 366.
(8) Yanagisawa, T.; Shimizu, T.; Kuroda, K.; Kato, C. *Bull. Chem. Soc. Jpn.* **1990**, *63*, 988.
(9) Kresge, C. T.; Leonowicz, M. E.; Roth, W. J.; Vartuli, J. C.; Beck, J. S. *Nature* **1992**, *359*, 710.
(10) Attard, G. S.; Glyde, J. C.; Goltner, C. G. *Nature* **1995**, *378*, 366.
(11) Tian, Z. R.; Tong, W.; Wang, J. Y.; Duan, N. G.; Krishnan, V. V.; Suib, S. L. *Science* **1997**, *276*, 926.
(12) Zhao, D.; Feng, J.; Huo, Q.; Melosh, N.; Fredrickson, G. H.; Chmelka, B. F.; Stucky, G. D. *Science* **1998**, *279*, 548.
(13) Joo, S. H.; Choi, S. J.; Oh, I.; Kwak, J.; Liu, Z.; Terasaki, O.; Ryoo, R. *Nature* **2001**, *412*, 169.
(14) Pai, R. A.; Humayun, R.; Schulberg, M. T.; Sengupta, A.; Sun, J.; Watkins, J. J. *Science* **2004**, *303*, 507.
(15) Zou, X. D.; Conradsson, T.; Klingstedt, M.; Dadachov, M. S.; O'Keeffe, M. *Nature* **2005**, *437*, 716.
(16) Wan, Y.; Zhao, D. *Chem. Rev.* **2007**, *107*, 2821.
(17) Warren, S. C.; Messina, L. C.; Slaughter, L. S.; Kamperman, M.; Zhou, Q.; Gruner, S. M.; DiSalvo, F. J.; Wiesner, U. *Science* **2008**, *320*, 1748.
(18) Deng, Y.; Yu, T.; Wan, Y.; Shi, Y.; Meng, Y.; Gu, D.; Zhang, L.; Huang, Y.; Liu, C.; Wu, X.; Zhao, D. *J. Am. Chem. Soc.* **2007**, *129*, 1690.
(19) Ma, G.; Yan, X.; Li, Y.; Xiao, L.; Huang, Z.; Lu, Y.; Fan, J. *J. Am. Chem. Soc.* **2010**, *132*, 9596.
(20) Tseng, W.; Chen, C.; Chiang, Y.; Ho, R.; Akasaka, S.; Hasegawa, H. *J. Am. Chem. Soc.* **2009**, *131*, 1356.
(21) Xue, J.; Henry, C.; Lee, J.; Vogt, B. D. *RSC Adv.* **2014**, *4*, 3675.
(22) Gutiérrez, L.; Hamoudi, S.; Belkacemi, K. *Catalysts* **2011**, *1*, 97.
(23) Wu, Z.; Li, W.; Webley, P. A.; Zhao, D. *Adv. Mater.* **2012**, *24*, 485.
(24) Tan, K. W.; Jung, B.; Werner, J. G.; Rhoades, E. R.; Thompson, M. O.; Wiesner, U. *Science* **2015**, *349*, 54.
(25) Lin, J.; Peng, Z.; Liu, Y.; Ruiz-Zepeda, F.; Ye, R.; Samuel, E. L.G.; Yacaman, M.; Yakobson, B. I.; Tour, J. M. *Nat. Commun.* **2014**, *5*, 5714.
(26) Song, D.-P.; Lin, Y.; Gai, Y.; Colella, N. S.; Li, C.; Liu, X.-H.; Gido, S.; Watkins, J. J. *J. Am. Chem. Soc.* **2015**, *137*, 3771.
(27) Song, D.-P.; Li, C.; Colella, N. S.; Lu, X.; Lee, J.-H.; Watkins, J. J. *Adv. Opt. Mater.* **2015**, *3*, 1169.
(28) Daga, V. K.; Anderson, E. R.; Gido, S. P.; Watkins, J. J. *Macromolecules* **2011**, *44*, 6793.
(29) Logunov, S. L.; Ahmadi, T. S.; El-Sayed, M. A.; Khoury, J. T.; Whetten, R. L. *J. Phys. Chem. B* **1997**, *101*, 3713.
(30) Song, D.-P.; Li, C.; Colella, N. S.; Xie, W.; Li, S.; Lu, X.; Gido, S.; Lee, J.-H.; Watkins, J. J. *J. Am. Chem. Soc.* **2015**, *137*, 12510.
(31) Moon, J. H.; Seo, J. S.; Xu, Y.; Yang, S. *J. Mater. Chem.* **2009**, *19*, 4687.
(32) Mayer, K. M.; Hafner, J. H. *Chem. Rev.* **2011**, *111*, 3828.
(33) Bolton, J.; Bailey, T. S.; Rzayev, J. *Nano Lett.* **2011**, *11*, 998.
(34) Deng, Y.; Wei, J.; Sun, Z.; Zhao, D. *Chem. Soc. Rev.* **2013**, *42*, 4054.

DOI: 10.1021/jacs.6b06947
J. Am. Chem. Soc. 2016, 138, 13473−13476